Objective functions for the blade shape optimization of a cross-flow tidal turbine under constraints

Karla RUIZ-HUSSMANN, Pierre-Luc DELAFIN, Cyrille BONAMY, Yves DELANNOY, Dominique THÉVENIN and Stefan HOERNER

Abstract—**Hydro-kinetic cross-flow tidal turbines (CFTT) are omni-directional and offer higher area-based power density compared to horizontal-axis tidal turbines, making them very attractive for tidal energy exploitation. However, the rotating motion around the vertical axis results in continuously varying angles of attack, causing alternating loads, which may lead to fatigue failure and structural damage. The OPTIDE Project addresses these challenges by implementing intracycle blade pitching to individually control the angle of attack, increasing the power coefficient C_P and reducing structural loads. For this purpose a Darrieus turbine is designed with embedded actuators in each blade. Firstly a blade shape optimization will be conducted to fit the actuator at the quarter-chord position while ensuring sufficient thickness. The optimization procedure couples Computational Fluid Dynamics (CFD) with a Genetic Algorithm. The employed optimizer OPAL++ sets ten variables for each individual, which describe the hydrofoil shape, length and tip speed ratio (TSR). A smooth hydrofoil shape is generated from the variables, followed by an automatic mesh generation. Subsequently, numerical simulations of each individual at the desired TSR are conducted, while keeping the blade pitch angle constant. Simulation results provide the C_P and stress acting on the turbine blades, which are the two optimization objectives (maximize C_P while minimizing stress). This process is repeated during the optimization, aiming to determine the most suitable blade shape, that fits the actuator, and operating point (TSR) in a trade-off between C_P and structural loads. This will lead to the increase of efficiency and a longer turbine lifetime.**

Index Terms—**Cross-flow tidal turbine, active variable pitch, optimization, CFD**

I. Introduction

In order to reduce the emissions of greenhouse gases and thus mitigate the climate change, a transition from fossil to renewable energies is urgently needed. Among the wide range of renewable energies, including solar, wind and hydropower, the latter stands out for its ability to remain unaffected by short-term weather changes and can thus be a reliable energy source. Conventional hydropower has made a notable contribution to the generation of renewable energies by covering up to 4476 TWh of the world wide energy consumption in 2020 as stated in the renewable energy statistics 2022 from the *International Renewable Energy Agency* (IRENA) [1]. Nonetheless, in order to harness the potential energy of the water, typical hydroelectric power plants require a sufficiently large hydraulic head, commonly achieved by using supporting structures such as dams, which impact the local ecosystem by creating a barrier in natural waterways. Besides this, most of the global locations are already being exploited, making it difficult to expand the energy production using conventional hydropower [2].

Recognizing the aforementioned limitations of conventional hydropower, research has been focusing on alternative solutions such as harnessing the vast potential of ocean energy. Analyses of IRENA project that until 2030 up to 10 GW of ocean energy could be installed worldwide [3]. Nevertheless, as of 2022 the installed capacity of marine energy corresponded to only 524 MW [4], showing the significant potential in the ocean energy field.

The sector of ocean energy can be classified by the various technologies, including tidal barrage, tidal stream and wave energy, among others. Of these, tidal barrage is the most commonly employed technology, followed by tidal stream, as stated by IRENA 2020 [3]. The tidal barrage technology captures the potential energy created by the difference in height between low and high tide and must therefore be built close to the coasts, limiting the number of possible sites worldwide. Another drawback of this technology is that, similar to conventional hydropower, additional supporting structures are required, resulting in greater environmental impacts. Compared to this, in a similar manner to wind turbines, the tidal stream technology only uses the kinetic energy of the tidal current, and can therefore be positioned in open waters without needing extensive additional structures, making them more environmentally friendly and additionally raising the local acceptance as it may be perceived as less disruptive by the local population (Holzman 2007 [5] and Müller *et al.* [6].

These hydro-kinetic tidal turbines are usually catego-

This work is part of the OPTIDE project and has been supported by the Deutsche Forschungsgemeinschaft (DFG (FKZ: 457325924)) and the labex Tec21 Investissements d'avenir - agreement n°ANR-11-LABX-0030.

K. Ruiz-Hussmann, D. Thévenin and S. Hoerner are at the Laboratory of Fluid Dynamics and Technical Flows, Institute of Fluid Dynamics and Thermodynamics, Otto von Guericke University Magdeburg, Universitätsplatz 2, 39106 Magdeburg, Germany. The first author works also at the Univ. Grenoble Alpes, CNRS, Grenoble INP, LEGI, 38000 Grenoble, France (e-mail: karla.ruiz@ovgu.de, thevenin@ovgu.de, hoerner@ovgu.de).

P.-L. Delafin, C. Bonamy and Y. Delannoy are at the Univ. Grenoble Alpes, CNRS, Grenoble INP, LEGI, 38000 Grenoble, France (e-mail: pierre-luc.delafin@univ-grenoble-alpes.fr, cyrille.bonamy@univ-grenoble-alpes.fr, yves.delannoy@grenoble-inp.fr).

Digital Object Identifier:
https://doi.org/10.36688/ewtec-2023-252

rized into axial turbines, often known as horizontal axis turbines (HAT), and vertical axis turbines. The latter, also referred to as cross-flow tidal turbines (CFTT), feature their central axis perpendicular to the direction of the incoming flow and are the technology to be considered in this study. CFTTs feature many advantages over HAT, including that they are omni-directional. Due to the positioning of the central axis they are insensitive to the flow direction, eliminating the need for a yawing system and making them perfectly suitable for harnessing energy of tidal currents as stated by Abbaszadeh *et al.* 2019 [7] and Delafin *et al.* 2021 [8]. Another main advantage is that CFTTs feature higher area-based power density in comparison to HAT as shown by Dabiri 2011 and others [9]–[11].

Despite the mentioned advantages of cross-flow tidal turbines, there are still some drawbacks and challenges remaining. One of these is, that due to the rotating motion around the vertical axis, each blade experiences continuous variations of the angle of attack during one revolution. This may cause dynamic stall as well as high alternating loads, which lead to fatigue failure, lower lifetime and even structural damage of the turbine, as reported by Kirke & Lazauskas 2011 [12], Abbaszadeh *et al.* 2019 [7] and Balduzzi *et al.* 2021 [13]. For the same reason, CFTTs additionally feature a lower overall turbine efficiency compared to HAT (Kirke & Lazauskas 2011 [12], Delafin *et al. 2021* [8] and Hoerner *et al.* 2021 [14]).

As mentioned before, it can clearly be seen, that there are still some challenges for CFTTs which need to be overcome in order to reach full potential of these turbines. Different propositions can be found in literature in order to increase turbine efficiency while trying to reduce blade stall. These approaches include adapting and optimizing the blade shape, as presented by Mohamed 2012 [15], Daróczy *et al.* 2018 [16] and Hashem & Mohamed 2018 [17] for a wind turbine and by Yang & Shu 2012 [18] for a helical tidal turbine, or changing typical geometrical design parameters, such as the amount of blades. Still, the three-bladed turbine is generally found to be the best solution as reported by Kirke & Paillard 2011 [12].

Another very promising approach to increase turbine efficiency and reduce stall is blade pitching, which allows to change the angle of attack of the turbines blade during one rotation. Blade pitching can be conducted in a passive or active manner. During passive pitching the blade is allowed to move freely, whereas active pitching mechanically changes the angle of attack of each blade. Several studies have been conducted for passive blade pitching, e.g. by Hantoro *et al.* 2011 [19], Lazauskas & Kirke 2012 and others [20], [21], as well as for active pitching by Hwang *et al.* 2009 [22], Branger *et al.* 2018 [23] or Delafin *et al.* 2021 [8] among others [7], [24], [25]. Kirke & Lazauskas 2011 [12] and 2012 [20] suggest that the latter has a great potential to increase turbine efficiency while reducing stall and alternating loads on the turbine. However, only few experimental studies have been conducted on active blade pitching, for example by Hwang *et al.* 2009 [22] or Liang *et al.* 2016 [25], giving less promising results as the support structure of the pitching mechanism causes unfavorable hydrodynamics and, therefore, reduces turbine overall efficiency.

Fig. 1. 3D Model of the CFTT developed in the OPTIDE project

Summarizing, it is still necessary to conduct further research on the implementation of the blade pitching mechanism. The OPTIDE project described in this study, aims to investigate the effect of pitching blades on CFTTs by coupling experimental and numerical research. The objective of the project is to develop a three-bladed CFTT flume model with a blade-embedded pitching mechanism in order to experimentally optimize the pitching trajectory of each blade. In Fig. 1 the 3D model of the OPTIDE Turbine can be seen. Due to restrictions given by the size of the flume tank used in this project, the turbine has been designed with a diameter D of 400 mm as well as a blade height H of 400 mm. The three blades of the turbine are connected with the shaft through two blade supports, which are located at the top and bottom of the blades. This setup allows to position the pitching actuators inside of each blade, hiding them from the flow and therefore reducing drag. A global description of the project and details of the experimental optimization approach for the blade pitch trajectory are given by Hoerner *et al.* 2023 [26].

In order to fit the actuator inside the blade while complying with necessary scales and geometrical constraints it is indispensable to find a suitable blade shape for the turbine. As mentioned before, similar studies have been conducted before with the purpose of finding blade shapes that improve the turbines efficiency,

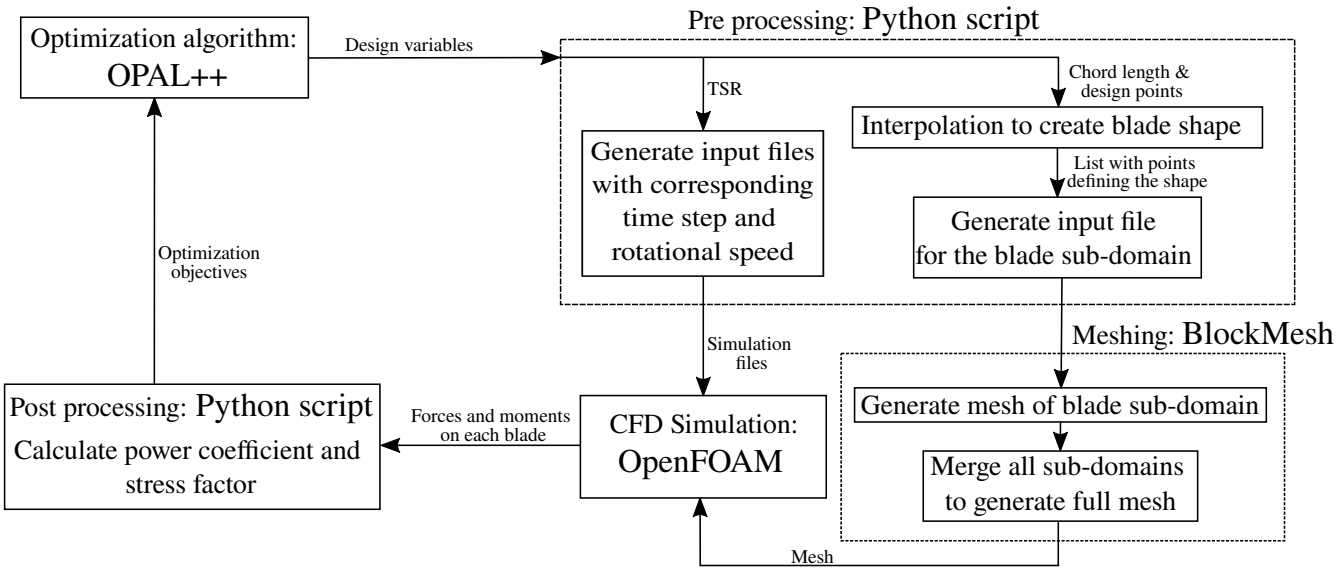

Fig. 2. Flowchart of the optimization loop showing the main programs used and the tasks completed in each step.

such as presented for example by Mohamed 2012 [15], Carrigan *et al.* 2012 [27], Bedon *et al.* 2016 [28], Daróczy *et al.* 2018 [16] and Hashem & Mohamed 2018 [17]. However, these studies were performed in order to improve the aerodynamic efficiency of vertical-axis wind turbines. It can not be assumed, that the found shapes are optimal as well for CFTTs, as these have different operating points (lower tip speed rations and thus higher angles of attack). Additionally, the proposed shapes do not guarantee the fitting of the actuator at a quarter-chord position and they do not take into account the structural loads, which truly affect turbine lifetime. For this reason, it is necessary to conduct a dedicated blade shape optimization in order to find a suitable blade design, constrained by the actuator size, and the corresponding optimal operating point, defined by the tip speed ratio (TSR). The objectives of the optimization include (1) maximizing the power coefficient C_P and additionally (2) minimizing the structural loads as quantified by the stress within the blade.

In this paper the methodology employed for the blade shape optimization of the OPTIDE project is presented. The main focus is set on the definition of the objective functions, as it introduces a novel approach not yet found in existing literature.

II. Methodology

Aim of the optimization is to find the optimal blade shape that fits the actuator and the best operating point in order to maximize the power and minimize the structural loads on the turbine. The operating point of turbines is defined by the tip speed ratio (TSR), which describes the ratio between the tangential velocity of the turbine, given by the angular velocity ω multiplied by the turbine radius R, and the velocity of the incoming flow v_∞:

$$TSR = \frac{\omega R}{v_\infty} \tag{1}$$

The subsequent section provides a detailed description of the applied methodology for the blade shape optimization, which consists of computational fluid dynamics (CFD) coupled with evolutionary algorithms. The optimization process can be subdivided in several components: the optimization software, the blade shape and mesh generation, the CFD simulation and the post processing of the results in order to calculate the optimization objectives. Fig. 2 shows a flowchart of the optimization loop and the interaction between the different components.

The main component of the optimization process is the employed optimization algorithm as it acts like a higher-level process that executes and evaluates the sub-tasks conducted during the optimization. Many different algorithms exist in order to solve optimization problems. In the present study, a Genetic Algorithm has been selected as they are known for their efficiency to find a global optimum, instead of being limited by converging towards local maxima as stated by Ouyang *et al.* 2006 [29] and Shahrokhi & Jahangirian 2007 [30]. For this research, the optimization tool *OPtimization Algorithm Library ++ (OPAL++)* developed at the Otto von Guericke University Magdeburg and firstly introduced by Daróczy *et al.* 2014 [31], has been employed. This algorithm has already been successfully used for many different single- as well as multi-objective optimization problems by Daróczy *et al.* 2014 [31] and 2018 [16], Abbaszadeh *et al.* 2019 [7], Kerikous & Thévenin 2019 [32], Mansour *et al.* 2020 [33] and Das *et al.* 2022 [34].

As mentioned before, in the presented work a multi-objective optimization will be conducted, with the aim of maximizing the power coefficient C_P and reducing the stress in the turbine blades during one revolution. The exact definition of the objective functions will be presented later in section II-C. During the optimization process a minimum of 500 different individuals will be analyzed. For each of these individuals the optimization algorithm *OPAL++* sets ten different design variables, including the TSR, the chord length and

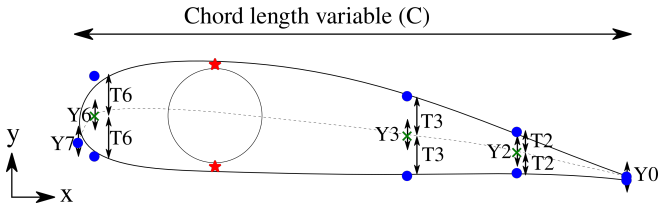

Fig. 3. Definition of the points that determine the hydrofoil shape. Points marked with red stars are fixed, whereas blue circles change for each individual

TABLE I
VARIABLES SET BY THE OPTIMIZER AND THEIR MINIMAL AND MAXIMAL VALUES

Variable	Minimal Value	Maximal Value
C	60 mm	90 mm
TSR	1.5	3.0
$Y0$	-10.0 mm	0.0 mm
$Y2$	-10.0 mm	0.0 mm
$Y3$	-10.0 mm	0.0 mm
$Y6$	-10.0 mm	0.0 mm
$Y7$	-10.0 mm	0.0 mm
$T2$	2.0 mm	5.2 mm
$T3$	2.0 mm	5.2 mm
$T6$	2.0 mm	6.5 mm

eight points which define the hydrofoil shape (see Fig. 3). In section II-A the generation of the blade shape is described in detail. In order to keep the blade shape, size and TSR in a range that makes sense for the given application, constraints are set for the different variables in the optimizer. Table I shows the ten design variables and the minimal and maximal values allowed. Additionally, five more constraints were imposed to exclusively permit the cambering of the blade in one direction and enforce a shape that becomes thinner towards the trailing edge. These constraints ensure that all considered shapes will be meaningful and could be really produced.

These variables are handed over to a *Python* script which generates a smooth hydrofoil shape, out of which a mesh is generated. Subsequently the CFD simulation of each individual follows. It will be performed on the cluster at the Laboratoire des Ecoulements Géophysiques et Industriels (LEGI) in Grenoble, France. The steps of the shape and mesh generation as well as the CFD simulations are further explained in section II-A and II-B. When the simulations are finished the results are exported to a *Python* script using the *FluidFoam package* developed at LEGI [35]. The objective functions of the optimization are calculated and passed back to the optimizer. Finally *OPAL++* evaluates the results of all the individuals and generates a new set of hydrofoil design parameters, derived from the best performing individuals by cross-over of the parental parameters for the offspring. Additionally a mutation is performed by the optimization algorithm in order to explore the entire possible design space while searching for a global optima. Thereupon the optimization loop starts again.

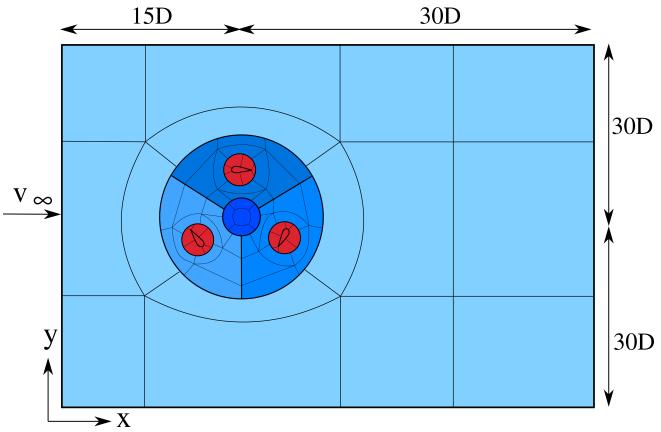

Fig. 4. Computational domain and block structure of the mesh. The blue blocks remain constant for each individual, the red blocks represent the individually generated meshes. Note that the image is not to scale

A. Shape and mesh generation

This subsection describes how the blade shape is generated from the given design parameters of the optimizer as well as the subsequent generation of the mesh. The blade shapes of each individual are initially defined by ten different points, which can be seen in Fig. 3. The two red points are fixed at the quarter chord position in order to protect the necessary thickness required for the pitching actuator. The coordinates of the blue points are variable for each individual and are defined as function of the chord length; they constitute the eight parameters set by the optimizer. These eight parameters are split into five values representing the y-coordinate of the camber line and three values for the thickness of the blade at three locations of the blade. The exact definition can be retrieved from Fig. 3.

The resulting ten points are processed by a *Python* script, which makes use of the *scipy* interpolation package to fit a Bézier curve and to generate a smooth hydrofoil. The output of the python script is a list of 2000 points that defines the blade shape. These points are then automatically written into a so-called dictionary file needed for the meshing utility.

In the present work the *OpenFOAM* toolkit (version 2212 from the ESI fork) is employed for the mesh generation and the CFD simulations. For the mesh generation the *blockMesh* utility has been chosen, as it allows to fully control the meshing process ensuring a high-quality two-dimensional structured hexahedral mesh for each individual. Fig. 4 shows the computational domain of the turbine as well as its block structure. It can be seen that the mesh consists of several parts, each highlighted in a different color. The parts highlighted in different shades of blue remain constant for all the individuals, while the red blocks, the so-called blade sub-domains, are meshed again for each individual. The blade mesh is constructed on the base of the *blockMesh* dictionary file mentioned before, which contains the list of points describing the blade shape. For the mesh it has been taken care to satisfy $y^+ \sim 1$ (the maximally measured value was 1.6) close to the blade wall for a fully resolved boundary layer accordingly to the requirements formulated by

Maître *et al.* 2013 [36]. Subsequently all different mesh components are joined together with the *mergeMesh* function of the *OpenFOAM* toolkit, resulting in a mesh with 121,000 cells.

After the mesh has been generated the *checkMesh* function of the *OpenFOAM* toolkit is employed in order to verify, that the automatically generated mesh complies with necessary requirements. The parameters have been customized in order to use only well defined meshes for accurate results in the process. If *checkMesh* fails, the individual automatically becomes invalid and will not be taken into account for further steps. A test was conducted in order to quantify the quality of the generated meshes. 200 different blade shapes and their corresponding meshes were created with the optimization tool and it was shown that less than 20% failed the mesh check.

B. CFD simulation

Following the completion of the meshing process, the CFD simulation is performed. The *pimpleFoam* solver of the *OpenFOAM* toolkit will be employed in order to solve the incompressible Unsteady Reynolds-Averaged Navier-Stokes (URANS) equations. The $k-\omega-$SST (Shear Stress Transport) turbulence model has been selected in order to accurately model the Reynolds Stresses.

At the inlet boundary the velocity of the incoming flow was set to v_∞ = 0.8 m/s, representing the flow velocity in the flume used for the experiments of the OPTIDE project. The turbulence intensity was set to 15% (k = 0.024 m^2/s^2), which dissipates to 0.27% at the location of 1D before the turbine (x = -1D, k = $7{\cdot}10^{-6}$ m^2/s^2). The pressure at the outlet boundary was set to 0 Pa. The chord-based Reynolds number features a wide range from Re = 24,000 to 287,500, due to the variable blade length (60 mm to 90 mm) and TSR (1.5 to 3.0) as well as the alternating relative speed $w = v_\infty + \omega R$. Additionally, the simulations were initialized by mapping the flow field of a fully converged reference simulation. Tests with a few cases showed that with this technique, the variation in C_P between two consecutive revolutions is around 5% lower than with standard (uniform) initialization, which leads to a faster convergence of each individual and reduces the calculation time by roughly 20%.

For each individual, ten turbine revolutions were simulated with a time step of 1°, which was determined through a time step independence study. Each simulation is carried out in parallel on 4 cores of the LEGI cluster, whereas 32 different cases were executed simultaneously on the cluster. The time needed in order to solve each case depends on the settings (blade shape and TSR) of each individual. However, the test case presented in section III required roughly 14 hours (56 CPU hours) to simulate ten turbine revolutions.

C. Objective functions

During the simulations, the forces and moments on each blade are saved for each time step. When the simulations are finalized the results are imported to the post processing *Python* script using the *FluidFoam package*, in order to calculate the two objective functions, (1) the cycle-averaged power coefficient C_P and (2) the cycle-averaged so called stress factor f_σ. Finally, these two values are handed over to the optimizer, which evaluates the results of all the individuals of one generation and generates a following set of individuals based on the fittest cases.

The first objective function in the present study is to maximize the power coefficient C_P, in order to find a suitable blade shape and TSR that increases the performance of the turbine. This objective function is typically used for similar optimization problems as conducted by Dároczy *et al.* 2018 [16], Hashem & Mohamed 2018 [17] and Kerikous & Thévenin (2019) [32]. The power coefficient C_P describes the ratio between the mechanical power generated by the turbine to the theoretical kinetic energy of the flow as shown in (2), with Q the turbine torque, ω the rotational speed of the turbine, ρ the water density, A the cross-section of the turbine and v_∞ the inflow velocity.

$$C_P = \frac{P_{\text{mech}}}{P_{\text{total}}} = \frac{Q \cdot \omega}{0.5 \cdot \rho \cdot A \cdot v_\infty^3} \tag{2}$$

As mentioned before, one of the biggest drawbacks of CFTTs is that they operate with a constantly changing angle of attack during one turbine revolution, causing high alternating loads, which leads to fatigue failure and even structural damage. To improve CFTTs turbines it is therefore not only necessary to increase their power output but also to decrease the high alternating loads experienced by the turbines blades. For this reason, in the present study it has been chosen to add a second objective function, that takes the occurring stresses in the blades – an indicator for fatigue – into account. In order to calculate the stresses in one blade during one revolution, the blade is modeled as a beam that is fixed at both ends (top and bottom of the turbine) with an evenly distributed load q given in N/m over the whole span of the blade. Fig. 5 (a) shows a schematic representation of the clamped beam with the evenly distributed load q represented in blue and the resulting forces ($F_{A,y}$, $F_{B,y}$) and moments (M_A, M_B) acting on the supports shown in red.

Due to the rotating motion of the turbine, the blade experiences a constantly changing angle of attack and therefore a varying relative speed during one revolution. As a result, the blade is subjected to alternating forces, which can be split up between the tangential and normal components. The tangential force F_t produces torque and is the driving force of the turbine, while the normal force F_n causes the structural loads [37]. For this reason the evenly distributed load q is derived from the normal force F_n acting on the entire span of the blade.

In order to calculate the internal stresses experienced by the blade, the first step is to calculate the forces and moments acting on the supports A and B. Following the method proposed by Luévanos Rojas & Montoya Ramírez 2014 [38] using the Bernouilli-Euler theory, fixed-ends forces and moments can be calculated with (3) and (4). In this model q is the evenly distributed

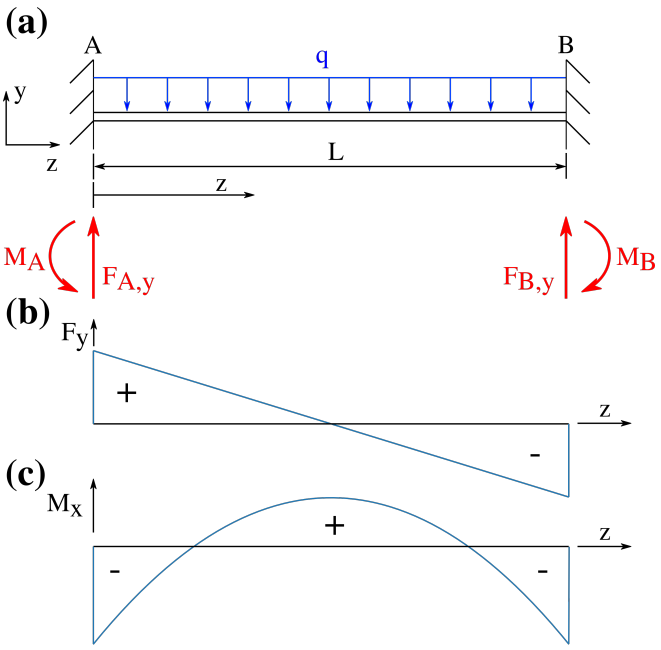

Fig. 5. (a) Schematic representation of the blade, modeled as a beam fixed on both ends with an evenly distributed load q over the span of the blade, shown in blue. Forces and moments acting on the supports are presented in red. Qualitative course of the internal forces (b) and moments (c) experienced by the presented beam setup

load caused by the normal force F_n (from the pressure acting on the blade) and l is the length of the blade, corresponding to 400 mm in the present study.

$$F_{\mathrm{A,y}} = F_{\mathrm{B,y}} = \frac{q \cdot l}{2} \tag{3}$$

$$M_\mathrm{A} = M_\mathrm{B} = \frac{q \cdot l^2}{12} \tag{4}$$

After determining the fixed-ends forces and moments, it is necessary to calculate the internal forces and moments experienced by the blade. In the presented system the blade will experience shear τ and bending stresses $\sigma_{\mathrm{b,x}}$ caused by an internal shear force $F_{\mathrm{q,y}}$ and a bending moment $M_{\mathrm{b,x}}$, respectively. For this reason the latter shall be determined as stated in (5) and (6), with z being the location of the blade on which the force and moment shall be calculated:

$$F_{\mathrm{q,y}} = q \cdot (\frac{l}{2} - z) \tag{5}$$

$$M_{\mathrm{b,x}} = \frac{q}{2} \cdot (l \cdot z - z^2 - \frac{l^2}{6}) \tag{6}$$

Fig. 5(b) and (c) display the course of the internal forces and moments qualitatively over the span of the blade respectively. It can be seen, that the magnitude of both values are highest at the clamped ends of the blade ($z = 0$ mm and $z = 400$ mm). Therefore, it is only necessary to calculate $F_{\mathrm{q,y}}$ and $M_{\mathrm{b,x}}$ at $z = 0$ mm or $z = 400$ mm during the optimization process. In the study at hand $z = 0$ mm has been chosen. Afterwards the shear τ and bending stresses $\sigma_{\mathrm{b,x}}$ can be calculated with (7) and (8) accordingly, where A is the cross-section of the blade and W is the section modulus.

$$\tau = \frac{F_{\mathrm{q,y}}}{A} \tag{7}$$

$$\sigma_{\mathrm{b,x}} = \frac{M_{\mathrm{b,x}}}{W} \tag{8}$$

The blades employed for the experimental turbine of the OPTIDE project are 3D printed using synthetic resin. The pitching actuators embedded in the blades have a diameter of 12 mm. However, the shaft connecting the servomotors with the blade support structure has a diameter of 6 mm. It is therefore expected, that the 6 mm shaft has to be able to support the alternating loads acting on the blades. Parallel finite-element-analysis on the flume model performed by Bennecke *et al.* 2022 [39] & 2023 [40] are in accordance with this assumption. For this reason it has been chosen to use the section modulus W and the area A of a circle with a diameter D_{motor} of 6 mm to calculate the stresses:

$$A = \frac{\pi \cdot D_{\mathrm{motor}}^2}{4} \tag{9}$$

$$W = \frac{\pi \cdot D_{\mathrm{motor}}^3}{32} \tag{10}$$

In such cases, where a fixed beam undergoes both shear and bending stress, the shear stresses τ are generally considerably smaller than the bending stresses $\sigma_{\mathrm{b,x}}$ and can therefore be neglected. This applies when the beam length is significantly larger than the beam thickness [41], [42], which is the case in the present study. Therefore, only the bending stresses $\sigma_{\mathrm{b,x}}$ will be taken into account.

To take into account the alternating loads acting on the blade, which periodically repeat every turbine turn, the bending stress is calculated for each time step (1° steps) of the last (tenth) revolution. The fatigue limit is often illustrated with the help of the Smith diagram, where the minimal and maximal stresses are plotted against the mean stress, taking into account static and dynamic fatigue as explained by Niemann *et al.* 2019 [41] or Wittel *et al.* 2015 [43]. As the minimal and maximal stresses (the amplitude of the stress $\sigma_{\mathrm{amplitude}}$) are displayed against the mean stress σ_{mean}, it can be concluded that both values are equally important for the fatigue strength. For this reason both values are to be considered for the second objective function, the so-called stress factor f_σ, of the optimization process. f_σ is determined by the sum of $\sigma_{\mathrm{amplitude}}$ and σ_{mean} as stated in (13).

For the optimization f_σ is to be minimized in order to raise the possible turbine lifetime and to allow for material saving with a load adapted rotor design. The amplitude $\sigma_{\mathrm{amplitude}}$ and the mean stress σ_{mean} of periodical loads are calculated as stated in (11) and (12), where $\sigma_{\mathrm{b,x,max}}$ is the maximal experienced bending stress during the last revolution of the turbine and $\sigma_{\mathrm{b,x,min}}$ the minimal stress.

$$\sigma_{\mathrm{amplitude}} = \frac{\sigma_{\mathrm{b,x,max}} - \sigma_{\mathrm{b,x,min}}}{2} \tag{11}$$

$$\sigma_{\mathrm{mean}} = \frac{|\sigma_{\mathrm{b,x,max}}| + |\sigma_{\mathrm{b,x,min}}|}{2} \tag{12}$$

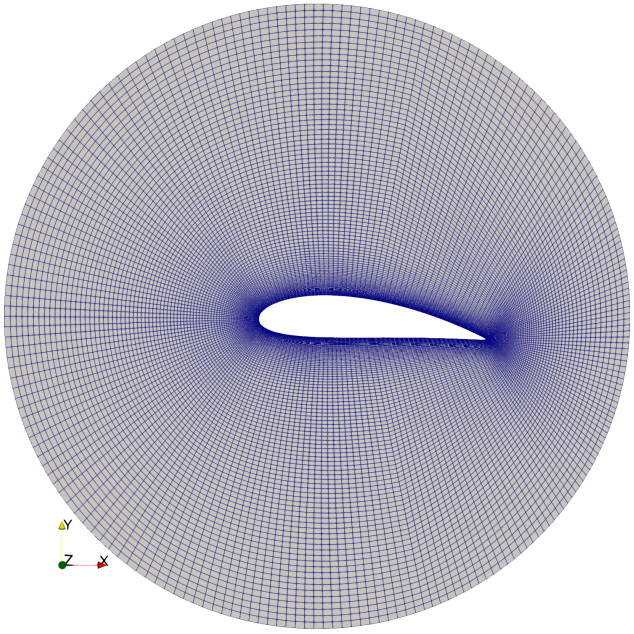

Fig. 6. Mesh of the blade domain for a NACA 0018 blade with a chord length of 75 mm, where the mean line has been projected to the diameter of the turbine

$$f_\sigma = \sigma_{\text{amplitude}} + \sigma_{\text{mean}} \tag{13}$$

III. Preliminary results

In the following section some preliminary results of the ongoing optimization will be presented. In order to check that the setup of the CFD simulation, the mesh generation and the calculation of the objective functions works correctly during the optimization a preparatory case has been created and established as the reference case. The blade shape employed for this purpose consisted of a NACA 0018 foil with a chord length of 75 mm, whose mean line has been projected to a circle of same diameter as the turbine (400 mm) to create a cambered airfoil (see Fig. 6). This reference case has been used to conduct the mesh sensitivity and time step sensitivity studies, leading to a final time step of 1° and a mesh with 121,000 cells. Fig. 6 shows the final mesh around the blade domain of the projected NACA 0018 foil.

For this geometry CFD simulations with the same parameters presented in section II-B and a $TSR = 2.25$ were conducted. As mentioned before, the case was run on 4 cores of the LEGI cluster and needed around 14 hours to simulate ten turbine revolutions. Both objective functions were calculated for the tenth revolution and resulted in a $C_P = 0.3044$ and $f_\sigma = 97.53$ MPa. For this case the difference of the C_P from the ninth to the tenth revolution was calculated, showing that the value fluctuated by less than 1%, which is the convergence criteria chosen for the present study.

Additionally, the shear and bending stresses (τ and $\sigma_{b,x}$) at the location $z = 0$ mm were plotted for the last revolution of the turbine. The course of the stresses over one rotation can be found in Fig. 7. It can clearly be seen, that the shear stresses are significantly

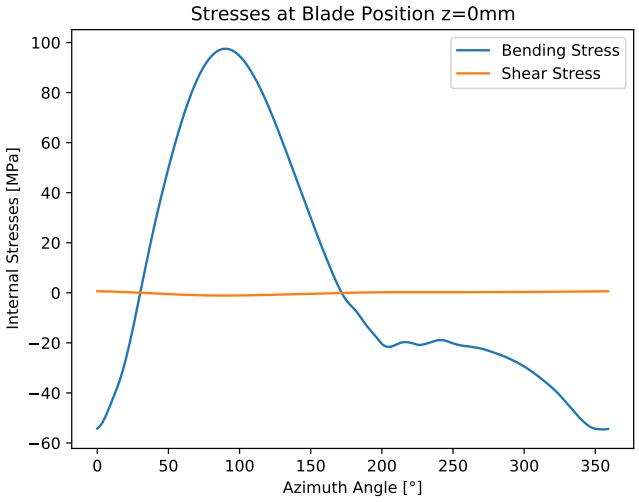

Fig. 7. Shear and bending stresses at the end of the blade ($z = 0$ mm plotted over the tenth revolution of the reference case

smaller than the bending stresses, confirming that it is reasonable to neglect the shear stress in the calculation of our objective function.

IV. Conclusion

The OPTIDE project aims at studying the effect of blade pitching on CFTTs. For this purpose a three-bladed CFTT experimental flume model with blade-embedded pitching mechanism will be developed. In order to fit the actuators inside each blade, it is necessary to find a suitable blade shape. Therefore, a blade shape optimization under this constraint is first conducted. Aim of the optimization process is to find the optimal operating point and a suitable blade shape that allows to fit the actuator at the quarter-chord position, while maximizing turbine performance (C_P) and minimizing the loads acting on the blades (f_σ). *OPAL++* has been chosen as the optimization algorithm, which sets the ten variables of the design space, defining the TSR and the blade shape, for each individual. A *Python* script generates a smooth hydrofoil shape and writes the dictionary file needed to generate a mesh using the *blockMesh* utility. Afterwards a 2D CFD simulation is conducted for each individual using *OpenFOAM*. The resulting moments and forces on the blades are calculated by *OpenFOAM* and imported to the post processing *Python* script, which calculates the cycle-averaged values for C_P and f_σ for the objective space. The optimizer evaluates the results and defines a new offspring generation using cross-over and mutations providing a set of variables for each individual on the base of the best performing individuals from the parent generation. This is repeated until the optimization converges defining optimal blade shapes for the CFTT forming a Pareto front.

In the presented paper the methodology employed for the multi-objective optimization is presented. The first objective function is to maximize the performance, i.e., the C_P of the turbine. The second objective function aims to take into account the alternating loads experienced periodically by the blades during one revolution

of the turbine. For this reason the stress factor based on the function f_σ has been developed, which includes both the mean value of the resulting stresses in the blade as well as the amplitude with which the stresses occur. With these functions a blade shape is to be found, which not only increases the performance of the turbine, but additionally reduces loads. This will help reducing the fatigue strength of the turbine, leading to a longer lifetime. Additionally a load-adapted design will allow for material savings, providing a lightweight and dynamic rotor.

The employed methodology is suitable for the presented application as the chosen objective functions do not only aim to increase the turbines efficiency, but to also decrease the experienced stress by the turbines blades. This is a new approach, which has not yet been found as such in literature. Additionally to that, by choosing a genetic algorithm it is possible to efficiently explore the design space while finding a global optimum. However, the considered range of the chord-based Reynolds number (Re = 24,000 to 287,500) lies in the transition between laminar and turbulent flow, which is difficult to reproduce in CFD with the chosen turbulence model.

After the optimization has been run, the blade shapes, which are eligible for the OPTIDE project, will be identified and implemented in the fume model. These blade shapes shall then be tested experimentally and compared with the experimental results of the reference case (projected NACA 0018) in order to check whether the results of the optimization are reasonable. Thereupon the pitching actuators will be implemented into the blades to conduct the experimental optimization of the pitching law, which is the main aim of the OPTIDE project.

REFERENCES

[1] IRENA, "Renewable energy statistics 2022," International Renewable Energy Agency, Tech. Rep., 2022.

[2] M. Balmer and D. Spreng, "Hydroelectric power," in *Future Energy*. Elsevier, 2008, pp. 193–209.

[3] IRENA, "Innovation outlook: Ocean energy technologies," International Renewable Energy Agency, Tech. Rep., 2020.

[4] ——, "Renewable capacity statistics 2023," International Renewable Energy Agency, Tech. Rep., 2023.

[5] D. C. Holzman, "Blue power: Turning tides into electricity," *Environmental Health Perspectives*, vol. 115, no. 12, dec 2007.

[6] S. Müller, V. Muhawenimana, G. Sonnino-Sorisio, C. A. M. E. Wilson, J. Cable, and P. Ouro, "Fish response to the presence of hydrokinetic turbines as a sustainable energy solution," *Scientific Reports*, vol. 13, no. 1, may 2023.

[7] S. Abbaszadeh, S. Hoerner, T. Maître, and R. Leidhold, "Experimental investigation of an optimised pitch control for a vertical-axis turbine," *IET Renewable Power Generation*, vol. 13, no. 16, pp. 3106–3112, nov 2019.

[8] P.-L. Delafin, F. Deniset, J. A. Astolfi, and F. Hauville, "Performance improvement of a darrieus tidal turbine with active variable pitch," *Energies*, vol. 14, no. 3, p. 667, jan 2021.

[9] R. Whittlesey, S. Liska, and J. Dabiri, "Fish schooling as a basis for vertical axis wind turbine farm design," *Bioinspiration & Biomimetics*, vol. 5, no. 3, p. 035005, 2010.

[10] J. O. Dabiri, "Potential order-of-magnitude enhancement of wind farm power density via counter-rotating vertical-axis wind turbine arrays," *Journal of Renewable and Sustainable Energy*, vol. 3, no. 4, p. 043104, jul 2011.

[11] I. Brownstein, M. Kinzel, and J. Dabiri, "Performance enhancement of downstream vertical-axis wind turbines," *Journal of Renewable and Sustainable Energy*, vol. 8, p. 053306, 2016.

[12] B. Kirke and L. Lazauskas, "Limitations of fixed pitch darrieus hydrokinetic turbines and the challenge of variable pitch," *Renewable Energy*, vol. 36, no. 3, pp. 893–897, mar 2011.

[13] F. Balduzzi, P. F. Melani, G. Soraperra, A. Brighenti, L. Battisti, and A. Bianchini, "Some design guidelines to adapt a darrieus vertical axis turbine for use in hydrokinetic applications," *E3S Web of Conferences*, vol. 312, p. 08017, 2021.

[14] S. Hoerner, S. Abbaszadeh, O. Cleynen, C. Bonamy, T. Maître, and D. Thévenin, "Passive flow control mechanisms with bioinspired flexible blades in cross-flow tidal turbines," *Experiments in Fluids*, vol. 62, no. 5, apr 2021.

[15] M. Mohamed, "Performance investigation of h-rotor darrieus turbine with new airfoil shapes," *Energy*, vol. 47, no. 1, pp. 522–530, nov 2012.

[16] L. Daróczy, G. Janiga, and D. Thévenin, "Computational fluid dynamics based shape optimization of airfoil geometry for an h-rotor using a genetic algorithm," *Engineering Optimization*, vol. 50, no. 9, pp. 1483–1499, jan 2018.

[17] I. Hashem and M. Mohamed, "Aerodynamic performance enhancements of h-rotor darrieus wind turbine," *Energy*, vol. 142, pp. 531–545, jan 2018.

[18] B. Yang and X. Shu, "Hydrofoil optimization and experimental validation in helical vertical axis turbine for power generation from marine current," *Ocean Engineering*, vol. 42, pp. 35–46, mar 2012.

[19] R. Hantoro, I. K. A. P. Utama, E. Erwandi, and A. Sulisetyono, "An experimental investigation of passive variable-pitch vertical-axis ocean current turbine," *Journal of Engineering and Technological Sciences*, vol. 43, no. 1, pp. 27–40, 2011.

[20] L. Lazauskas and B. Kirke, "Modeling passive variable pitch cross flow hydrokinetic turbines to maximize performance and smooth operation," *Renewable Energy*, vol. 45, pp. 41–50, 2012. [Online]. Available: https://www.sciencedirect.com/science/article/pii/S0960148112001395

[21] B. K. Kirke and B. Paillard, "Predicted and measured performance of a vertical axis wind turbine with passive variable pitch compared to fixed pitch," *Wind Engineering*, vol. 41, no. 1, pp. 74–90, nov 2016.

[22] I. S. Hwang, Y. H. Lee, and S. J. Kim, "Optimization of cycloidal water turbine and the performance improvement by individual blade control," *Applied Energy*, vol. 86, no. 9, pp. 1532–1540, sep 2009.

[23] H. Branger, B. Paillard, S. Roy, C. Luneau, E. Perrot, and D. Bourras, "Experimental and numerical study on a model of offshore vertical axis wind turbine with pitching blades," in *7th Conference on Bluff Body Wakes and Vortex-Induced Vibrations, BBVIV-7*, 2018.

[24] B. Paillard, J. Astolfi, and F. Hauville, "URANSE simulation of an active variable-pitch cross-flow darrieus tidal turbine: Sinusoidal pitch function investigation," *International Journal of Marine Energy*, vol. 11, pp. 9–26, sep 2015.

[25] Y. Liang, L. Zhang, E. Li, and F. Zhang, "Blade pitch control of straight-bladed vertical axis wind turbine," *Journal of Central South University*, vol. 23, no. 5, pp. 1106–1114, may 2016.

[26] S. Hoerner, R. Leindhold, S. Abbaszadeh, K. Ruiz-Hussmann, T. Bennecke, Z. Zhao, P. Joedecke, C.-T. Weber, P.-L. Delafin, C. Bonamy, and Y. Delannoy, "Experimental optimization environment for developing an intracycle pitch control in cross flow turbines," in *Proceedings of the 15th European Wave and Tidal Energy Conference, 3–7 September 2023, Bilbao*, 2023.

[27] T. J. Carrigan, B. H. Dennis, Z. X. Han, and B. P. Wang, "Aerodynamic shape optimization of a vertical-axis wind turbine using differential evolution," *ISRN Renewable Energy*, vol. 2012, pp. 1–16, jan 2012.

[28] G. Bedon, S. D. Betta, and E. Benini, "Performance-optimized airfoil for darrieus wind turbines," *Renewable Energy*, vol. 94, pp. 328–340, aug 2016.

[29] H. Ouyang, L. J. Weber, and A. J. Odgaard, "Design optimization of a two-dimensional hydrofoil by applying a genetic algorithm," *Engineering Optimization*, vol. 38, no. 5, pp. 529–540, jul 2006.

[30] A. Shahrokhi and A. Jahangirian, "Airfoil shape parameterization for optimum navier–stokes design with genetic algorithm," *Aerospace Science and Technology*, vol. 11, no. 6, pp. 443–450, sep 2007.

[31] L. Daróczy, G. Janiga, and D. Thévenin, "Systematic analysis of the heat exchanger arrangement problem using multi-objective genetic optimization," *Energy*, vol. 65, pp. 364–373, feb 2014.

[32] E. Kerikous and D. Thévenin, "Optimal shape of thick blades for a hydraulic savonius turbine," *Renewable Energy*, vol. 134, pp. 629–638, apr 2019.

[33] M. Mansour, K. Zähringer, K. D. Nigam, D. Thévenin, and G. Janiga, "Multi-objective optimization of liquid-liquid mixing in helical pipes using genetic algorithms coupled with computational fluid dynamics," *Chemical Engineering Journal*, vol. 391, p. 123570, jul 2020.

[34] T. K. Das, E. Kerikous, N. Venkatesan, G. Janiga, D. Thévenin, and A. Samad, "Performance improvement of a wells turbine through an automated optimization technique," *Energy Conversion and Management: X*, vol. 16, p. 100285, dec 2022.

[35] C. Bonamy, J. Chauchat, P. Augier, A. Mathieu, Q. Clemencot, R. Chassagne, G. Maurice, A. Gilletta, M. Renaud, and G. Gonçalves, "fluiddyn/fluidfoam: Release v0.2.3," 2022. [Online]. Available: https://doi.org/10.5281/zenodo.6453090

[36] T. Maître, E. Amet, and C. Pellone, "Modeling of the flow in a darrieus water turbine: Wall grid refinement analysis and comparison with experiments," *Renewable Energy*, vol. 51, pp. 497–512, mar 2013.

[37] S. Hoerner, S. Abbaszadeh, T. Maître, O. Cleynen, and D. Thévenin, "Characteristics of the fluid–structure interaction within darrieus water turbines with highly flexible blades," *Journal of Fluids and Structures*, vol. 88, pp. 13–30, jul 2019.

[38] A. Luévanos-Rojas and J. Montoya-Ramírez, "Mathematical model for rectangular beams of variable cross section of symmetrical linear shape for uniformly distributed load," *International journal of innovative computing, information & control*, vol. 10, no. 2, pp. 545–564, feb 2014.

[39] T. Bennecke, K. Ruiz-Hussmann, P. Joedecke, C.-T. Weber, P.-L. Delafin, C. Bonamy, and S. Hoerner, "A weak coupled model for the fluid-structure interactions on cross-flow tidal turbine model," in *The 8th European Congress of Computational Methods in Applied Sciences and Engineering ECCOMAS Congress 2022, Oslo, Norway*, 2022.

[40] T. Bennecke, S. Abbaszadeh, K. Ruiz-Hussmann, P. Joedecke, P.-L. Delafin, C.-T. Weber, and S. Hoerner, "A methodology to capture the single blade loads on a cross-flow tidal turbine flume model," in *Proceedings of the 15th European Wave and Tidal Energy Conference, 3–7 September 2023, Bilbao*, 2023.

[41] G. Niemann, H. Winter, B.-R. Höhn, and K. Stahl, *Maschinenelemente 1*. Springer Berlin Heidelberg, 2019.

[42] A. Böge and W. Böge, Eds., *Handbuch Maschinenbau*. Springer Fachmedien Wiesbaden, 2021.

[43] H. Wittel, D. Muhs, D. Jannasch, and J. Voßiek, *Roloff/Matek Maschinenelemente*. Springer Fachmedien Wiesbaden, 2015.